

Simulating X-ray bursts during a transient accretion event

Zac Johnston,^{1,2,3}* Alexander Heger,^{1,2,3,4,5} Duncan K. Galloway^{1,2,3}

¹*School of Physics and Astronomy, Monash University, Victoria 3800, Australia*

²*Monash Centre for Astrophysics (MoCA), Monash University, Victoria 3800, Australia*

³*Joint Institute for Nuclear Astrophysics - Center for the Evolution of the Elements, East Lansing, Michigan 48824, USA*

⁴*Department of Astronomy, Shanghai Jiao Tong University, Shanghai 200240, China*

⁵*School of Physics and Astronomy, University of Minnesota, Minneapolis, Minnesota 55455, USA*

Accepted XXX. Received YYY; in original form ZZZ

ABSTRACT

Modelling of thermonuclear X-ray bursts on accreting neutron stars has to date focused on stable accretion rates. However, bursts are also observed during episodes of transient accretion. During such events, the accretion rate can evolve significantly between bursts, and this regime provides a unique test for burst models. The accretion-powered millisecond pulsar SAX J1808.4-3658 exhibits accretion outbursts every 2 – 3 years. During the well-sampled month-long outburst of 2002 October, four helium-rich X-ray bursts were observed. Using this event as a test case, we present the first multi-zone simulations of X-ray bursts under a time-dependent accretion rate. We investigate the effect of using a time-dependent accretion rate in comparison to constant, averaged rates. Initial results suggest that using a constant, average accretion rate between bursts may underestimate the recurrence time when the accretion rate is decreasing, and overestimate it when the accretion rate is increasing. Our model, with an accreted hydrogen fraction of $X = 0.44$ and a CNO metallicity of $Z_{\text{CNO}} = 0.02$, reproduces the observed burst arrival times and fluences with root mean square (RMS) errors of 2.8 h, and $0.11 \times 10^{-6} \text{ erg cm}^{-2}$, respectively. Our results support previous modelling that predicted two unobserved bursts, and indicate that additional bursts were also missed by observations.

Key words: X-rays: bursts – stars: neutron – methods: numerical – pulsars: individual (SAX J1808.4-3658)

1 INTRODUCTION

Type I X-ray bursts are thermonuclear flashes in the accreted envelopes of neutron stars (Belian et al. 1976; Grindlay et al. 1976). In low-mass X-ray binaries (LMXBs), a mix of hydrogen and helium is transferred from a low-mass companion ($\lesssim 1 M_{\odot}$) to a neutron star via Roche-lobe overflow, forming an accretion disc which feeds nuclear fuel to the neutron star surface. The base of the accreted layer is buried deeper under new material and heated to the point of thermonuclear runaway (Woosley & Taam 1976; Joss 1977). The heat released by the rapid fusion of the accreted layer is observable as a burst of X-rays, lasting approximately 10–100 s. Fresh fuel is then accreted onto the ashes, and bursts recur within hours to days (for reviews, refer to Lewin et al. 1993; Strohmayer & Bildsten 2003; Galloway et al. 2008).

As each new layer of fuel is buried deeper, its hydrogen is steadily converted to helium via the beta-limited (hot)

CNO cycle. If the burst recurrence time is longer than the time to deplete hydrogen, the burst will ignite in a deep helium layer (Case 2, Fujimoto et al. 1981). This class of helium bursts reach Eddington luminosity (L_{Edd}) and exhibit photospheric radius expansion (PRE; Tawara et al. 1984; Lewin et al. 1984). Their lightcurves feature rapid onsets ($\lesssim 1$ s), broad plateaus (≈ 10 s), and short tails ($\lesssim 30$ s) due to the absence of extended *rp*-process burning.

Some X-ray burst systems, such as GS 1826-24 (Ubertini et al. 1999), accrete and produce bursts at a consistent rate. X-ray burst modelling to date has focused on stable accretion rates (e.g., Woosley et al. 2004; Heger et al. 2007; Keek & Heger 2011), and the dependence of burst properties on those rates (Lampe et al. 2016). Transient X-ray binaries, on the other hand, can remain dormant for years at a time and experience unstable surges of accretion known as outbursts. The addition of fresh material to the neutron star surface, as with stable accretors, can trigger series of X-ray bursts.

SAX J1808.4-3658 was the first accreting millisecond

*E-mail: zac.johnston@monash.edu

pulsar (AMXP) to be observed (in 't Zand et al. 1998; Wijnands & van der Klis 1998; Chakrabarty & Morgan 1998), and undergoes month-long outbursts every 2 – 3 years (e.g., Wijnands 2004; Galloway 2006; Hartman et al. 2008, 2009; Patruno & Watts 2012; Patruno et al. 2012, 2017). During the well-sampled outburst of 2002 October, four thermonuclear X-ray bursts were observed (Chakrabarty et al. 2003). Subsequent modelling determined these to be helium bursts (Galloway & Cumming 2006, hereafter G06). The bursts from this event have been proposed as a standard test case for numerical modelling (Case 2, Galloway et al. 2017).

Using a semi-analytic model with a one-zone ignition criterion (described in Cumming & Bildsten 2000), G06 matched models to the observed burst properties and constrained the distance of the system to 3.5 ± 0.1 kpc. In order to solve for the ignition conditions, the accretion rate was averaged between bursts. Because these models were computationally inexpensive, many thousands could efficiently explore parameter-space. Despite these advantages, the semi-analytic nature of the model lacks chemical and thermal inertia from one burst to the next.

To improve upon this modelling of the 2002 October outburst, we present a multi-zone simulation produced with the KEPLER code, which tracks the composition and thermal state of the envelope as the outburst evolves (Woosley et al. 2004). This is the first application of time-dependent accretion rates to multi-zone burst simulations, allowing us to capture the thermal and chemical inertia of the envelope throughout an accretion episode.

In Section 2, we describe the X-ray data from the 2002 October outburst, the code we used to simulate the bursts, the system parameters chosen for the simulation, how we constructed the accretion rate curve, and how burst properties were extracted for comparison with observations. In Section 3, we examine the effect that a time-varying accretion rate has compared to a constant rate, and compare the simulated burst properties with those observed, including times-of-arrival, fluences, and lightcurves. We summarise our results in Section 4, and discuss planned improvements to the model.

2 METHOD

2.1 Observational data

We used data from the 2002 October outburst taken with the Proportional Counter Array (PCA; Jahoda et al. 1996) and the All Sky Monitor (ASM; Levine et al. 1996) of the *Rossini X-ray Timing Explorer (RXTE)*. The PCA instrument is composed of five proportional counter units (PCUs) sensitive to photon energies of 2 – 60 keV. Two components of the PCA data were used: the persistent accretion flux, F_p (§. 2.5), and the time-resolved burst lightcurves, F_b (§. 3.2). The purpose of the ASM instrument is primarily to trigger alerts of transient events, and produces only low signal-to-noise data. It scans the sky every 90-minute orbit, and scans a given object roughly 5 – 10 times each day in 90-second exposures, from which 1-day average count rates are calculated.

The burst data were taken from the catalogue of Galloway et al. (2008), which was since re-analysed for the Multi

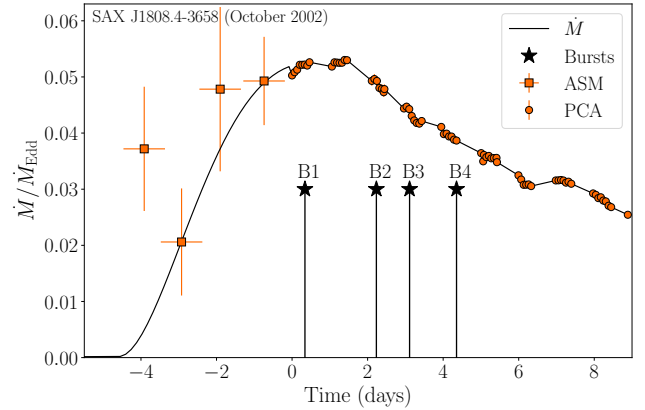


Figure 1. The accretion rate estimated from *RXTE* observations during the 2002 October outburst, as a fraction of the Eddington-limited rate ($\dot{M}_{\text{Edd}} = 1.75 \times 10^{-8} M_{\odot} \text{ yr}^{-1}$), assuming $d = 3.5$ kpc and ξ_p . Time has been zeroed to the start of PCA observations at MJD 52562.07296, and shown are the times of the four observed bursts. Linear interpolation has been used within the high-resolution PCA data, while a toy curve has been inserted as a stand-in for the rise, which was not observed by the PCA. Note that while ASM data have been plotted for reference, the rise curve was not explicitly fit to them.

INstrument Burst ARchive (MINBAR, in-development)¹. This re-analysis consisted of fitting absorbed blackbody models over the range 2.5 – 20 keV, with the neutral column density fixed at $n_H = 1.2 \times 10^{21} \text{ cm}^{-2}$ (Wang et al. 2001). Updated PCA response matrices (v11.7²) were used, and the recommended systematic error of 0.5 percent was adopted. Churazov weighting was employed to address the issue of low-count spectra in XSPEC (Dorman & Arnaud 2001). Deadtime was estimated using the Standard-1 mode data³, and the exposure time was then reduced by the deadtime correction factor, contributing an additional 25 – 30 percent to the photon flux at the burst peaks.

For the persistent flux (F_p), n_H was fixed, and updated response matrices and deadtime correction used, as with the burst data. Additionally, spectra were averaged over each observation separately for each PCU, excluding the burst times. Each spectrum was then fitted with one of a family of models, including blackbody+powerlaw or Comptonisation, often adopting a Gaussian component to model Fe K α emission around 6.4 keV. The models were then integrated over the range 3–25 keV, and the bolometric flux estimated.

2.2 Numerical method

To simulate the neutron star envelope during an accretion outburst, we used the 1D stellar hydrodynamics code KEPLER, which models a grid of Lagrangian zones in the radial direction (Weaver et al. 1978; Woosley et al. 2004). Each

¹ <http://burst.sci.monash.edu/minbar/>

² <http://heasarc.gsfc.nasa.gov/docs/xte/pca/doc/rmf/pccarmf-11.7/>

³ following the recipe at http://heasarc.gsfc.nasa.gov/docs/xte/recipes/pca_deadtime.html

zone, representing a spherically symmetric shell of stellar material, has its own isotopic abundances and thermal properties. Convection of heat and nuclei between zones is modelled using mixing length theory, where a time-dependent diffusion coefficient is set by the convective velocity (implementation described in Heger et al. 2000).

KEPLER uses an adaptive nuclear network that can track the reactions between more than 1,000 isotopes up to the proton drip line (Rauscher et al. 2002). Isotopes are automatically added and removed from the network as needed (Woosley et al. 2004). This allows us to efficiently model the β -limited CNO cycle, the 3α -process, the αp -process, and the rp -process (Cyburt et al. 2010, 2016).

KEPLER also uses an adaptive spatial grid, in which zones are actively split or combined at each timestep in order to maintain resolution of thermodynamic gradients. Multiple criteria govern this rezoning; we impose a minimum zone thickness of 10 cm, a surface zone mass of $\sim 10^{18}$ g, and the above-mentioned accretion depth of 10^{19} g. These were chosen to avoid needlessly creating large numbers of zones, while maintaining consistency of the resulting burst properties. The model described in § 3 has 71 initial zones, growing as mass is accreted to 122 zones at the time of the first burst, and to 174 zones by the end of the simulation.

The simulation domain extends from the NS photosphere to the deep ocean near the crust, covering column depths of $10^4 \lesssim y \lesssim 10^{12}$ g cm $^{-2}$ ($10^4 \lesssim \rho \lesssim 10^9$ g cm $^{-3}$). Accretion-driven heating in the crust from electron captures and pycnonuclear reactions is included as a luminosity at the base of the grid, L_{crust} . To set up the initial thermal state, the envelope is relaxed until thermal equilibrium is met between L_{crust} and the luminosity at the surface.

Nuclear reactions in the envelope are then switched on, and accretion is simulated by adding mass to the zone with an exterior mass coordinate of 10^{19} g ($y \approx 8 \times 10^5$ g cm $^{-2}$) at the rate \dot{M} , which may evolve with time. This depth is chosen to avoid unnecessary re-zoning at the surface. Above this, the accreted composition is advected, and heating from accretion and compression is included (Keek & Heger 2011).

The accreted fuel is composed of ^1H , ^4He , and ^{14}N , given by their mass fractions, X_0 , Y_0 , and Z_{CNO} , respectively. We choose ^{14}N for simplicity, because it is the most abundant CNO metal in solar material, and the hot-CNO cycle rapidly stabilises to equilibrium values of ^{14}O and ^{15}O .

2.3 General relativistic corrections

KEPLER performs calculations in the local NS frame using Newtonian gravity. This approximation is acceptable because the grid spans only a thin surface shell of the neutron star, over which the gravitational acceleration, g , varies by $\lesssim 2\%$. However, in order to compare results with observations, general relativity (GR) must be accounted for. Given a model Newtonian NS mass and radius (M , R), there are combinations of GR mass and radius (M_{GR} , R_{GR}) such that the surface gravity is equal under both regimes (refer to Appendix B of Keek & Heger 2011). In other words, the model can be considered equivalent to a neutron star with an ‘actual’ mass and radius of M_{GR} and R_{GR} . This is satisfied when

$$\frac{GM}{R^2} = \frac{GM_{\text{GR}}}{R_{\text{GR}}^2}(1+z), \quad (1)$$

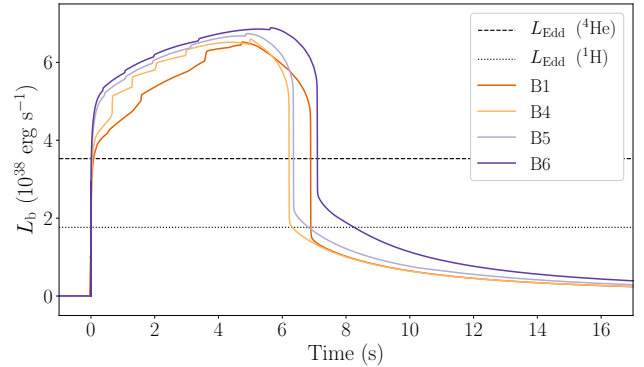


Figure 2. The raw simulated burst lightcurves, in the frame of the model. PRE bursts often exceed the Eddington luminosity in KEPLER, presumably because the physics of photospheric expansion and contraction are not accurately captured by the simple atmosphere, in addition to the lack of an outflow/wind mechanism. Low surface-resolution causes the visible steps during the peak, due to convection switching on as it spreads through these outer zones. To compare with the observations, we manually truncated the lightcurves at $L_{\text{Edd}}(^4\text{He})$ during analysis (§ 2.6; Fig. 4).

Table 1. Summary of parameters used in the model. Please note that these should not yet be considered best fit values to the system.

Quantity	Units	Description
g	1.86 10^{14} cm s $^{-2}$	Surface gravity
M	1.4* M_{\odot}	NS mass
R	11.2* km	NS radius
Q_b	0.3 MeV nucleon $^{-1}$	Crustal heating
X_0	0.44	Mass fraction
Z_{CNO}	0.02	Mass fraction
d	3.5 † kpc	Distance
ξ_p	1.1 †	Persistent anisotropy

* Effective GR-corrected values. Other combinations are still valid if they preserve g , but will alter $(1+z)$ and the conversion of model results to observable values (§ 2.3)

† Assumed values for inferring the accretion rate from persistent flux. Other combinations are still valid (§ 2.5)

where the gravitational redshift factor is

$$1+z = \frac{1}{\sqrt{1-2GM_{\text{GR}}/(c^2R_{\text{GR}})}}. \quad (2)$$

If we choose $M_{\text{GR}} = M$, the solutions are simplified, and the luminosity and time can be converted from the model’s Newtonian frame (L , t) to a distant observer frame (L_{∞} , t_{∞}) with

$$L_{\infty} = \frac{L}{1+z}, \quad t_{\infty} = t(1+z). \quad (3)$$

2.4 Model parameters

The model parameters are summarised in Table 1.

We adopt a gravitational mass of $M = M_{\text{GR}} = 1.4 M_{\odot}$ and a Newtonian model radius of $R = 10$ km, equivalent to $R_{\text{GR}} \approx 11.2$ km (Equation 1). This gives a surface gravity

of $g \approx 1.858 \times 10^{14} \text{ cm s}^{-2}$ and redshift of $1 + z \approx 1.259$. Note that the model can still be considered equivalent to any other pair of M_{GR} and R_{GR} that satisfy Equation 1.

To set up the initial envelope, the inner portion is composed of an iron substrate between column depths of $10^8 \lesssim y \lesssim 10^{12} \text{ g cm}^{-2}$ ($10^6 \lesssim \rho \lesssim 10^9 \text{ g cm}^{-3}$). Nuclear reactions are not calculated in the substrate, and it primarily acts as a thermal sink during bursts, representing the ocean of prior burst ashes. Above the substrate, between $10^4 \lesssim y \lesssim 10^8 \text{ g cm}^{-2}$ ($10^4 \lesssim \rho \lesssim 10^6 \text{ g cm}^{-3}$), we add ^4He to represent leftover fuel from the tail of the previous outburst. The size of this fuel layer could be varied in future studies.

Crustal heating from the inner boundary evolves with accretion rate according to $L_{\text{crust}} = Q_{\text{b}} \dot{M}$, where Q_{b} is the specific energy yield from reactions in the crust. We adopt a value of $Q_{\text{b}} = 0.3 \text{ MeV nucleon}^{-1}$, following the best-fitting model from G06. To initialise the envelope, we use this value with the long-term average accretion rate of $10^{-11} M_{\odot} \text{ yr}^{-1}$ (G06), until the layer is in thermal equilibrium.

The observed burst energetics indicate an average hydrogen composition of $\langle X \rangle \approx 0.1$ at the time of ignition (G06). The initial composition of the accreted fuel, however, is less well-constrained because there is a degeneracy between the X_0 and Z_{CNO} which result in the above $\langle X \rangle$ due to stable hot-CNO burning. For the purposes of this study, we choose a metallicity of $Z_{\text{CNO}} = 0.02$, following the best-fitting model from G06. Initial tests of X_0 in the range of $0.49 - 0.62$ (from the best-fitting 1σ range of G06) indicated that our models required a lower value to reproduce the observed burst timings. The model presented here has $X_0 = 0.44$, with the remaining composition being $Y_0 = 0.54$.

Accretion discs can cause anisotropies by scattering and blocking X-ray emission from the NS surface, changing the apparent luminosity to an observer (Fujimoto 1988; He & Keek 2016). The strength of the anisotropy is dependent on i , the inclination of the binary system to the observer's line-of-sight. The inclination is typically poorly constrained in LMXBs, with the value for SAX J1808.4-3658 inferred to be $50^\circ \lesssim i \lesssim 80^\circ$ (Chakrabarty & Morgan 1998; Wang et al. 2001; Bildsten & Chakrabarty 2001; Ibragimov & Poutanen 2009). The effect is represented as a scaling factor, ξ , which we include in the conversion between the model luminosity and the observed flux, given by

$$L = 4\pi d^2 \xi F. \quad (4)$$

Independent factors are used for the persistent emission (ξ_{p}) and the burst emission (ξ_{b}), because the emitting region is not necessarily the same for both mechanisms. We used ξ_{p} when calculating \dot{M} from persistent flux, and ξ_{b} when calculating the burst flux from the model burst luminosity.

2.5 Accretion history

We inferred the accretion history of the 2002 October outburst from the observed persistent flux, F_{p} . Accretion onto the surface generates a luminosity of

$$L_{\text{acc}} = -\dot{M}\phi \quad \text{erg s}^{-1}, \quad (5)$$

where $\phi = -c^2 z / (1+z) \approx -0.2 c^2$ is the gravitational potential at the NS surface. Using Equations 3 and 4, the accretion

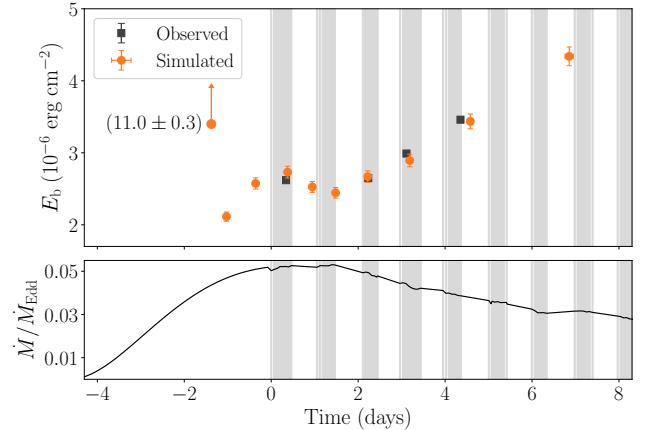


Figure 3. Upper panel: Fluence, E_{b} , of the modelled burst sequence against the four observed bursts. Lower panel: the time-varying accretion rate over the event, as a fraction of the Eddington-limited accretion rate. The vertical grey bands indicate when the telescope was collecting data. Note that extra bursts predicted by the model fall outside these observing windows. As is typical for KEPLER models, the first burst was anomalously energetic, and its off-axis E_{b} is indicated next to the arrow. The fluences have been calculated from the burst energy with the scaling factor $c_2 = 4\pi d^2 \xi_{\text{b}} \approx 1.05 \times 10^{45} \text{ cm}^2$, chosen such that the RMS error with observations is minimised (§ 3.2).

rate in the model frame is then given by

$$\dot{M} = \frac{-4\pi d^2 \xi_{\text{p}} (1+z)}{\phi} F_{\text{p}}. \quad (6)$$

We can rewrite this expression in terms of a conversion constant,

$$\dot{M} = \frac{-c_1 (1+z)}{\phi} F_{\text{p}}, \quad c_1 = 4\pi d^2 \xi_{\text{p}}. \quad (7)$$

For this model, we chose $d = 3.5 \text{ kpc}$ (G06), and $\xi_{\text{p}} = 1.1$, which is the predicted anisotropy factor for an inclination of $55^\circ \lesssim i \lesssim 60^\circ$ (Fig. 8 of He & Keek 2016). Thus, we have a conversion constant of $c_1 \approx 1.612 \times 10^{45} \text{ cm}^2$. Note that this model is still applicable to other combinations of d and ξ_{p} that preserve c_1 .

PCA observations did not commence until the peak of the outburst, and so the precise onset of accretion is ambiguous. For reference, the rise of the subsequent 2005 June outburst was observed to last 5 days (Hartman et al. 2008). For the 2002 October outburst, only 1-day average count rates from the ASM are available, constraining the rise length to 4–5 days. With these considerations, we substituted a toy curve for the accretion rise with a length of approximately 4 days. We expect that differences in the chosen onset should primarily influence the first burst or two, which likely went unobserved (§ 3.2). Nevertheless, we plan to investigate the effect of rise length and shape in a future study.

Combined with the PCA data and Equation 6, we thus obtained a continuous $\dot{M}(t)$ curve for input to the model (Fig. 1).

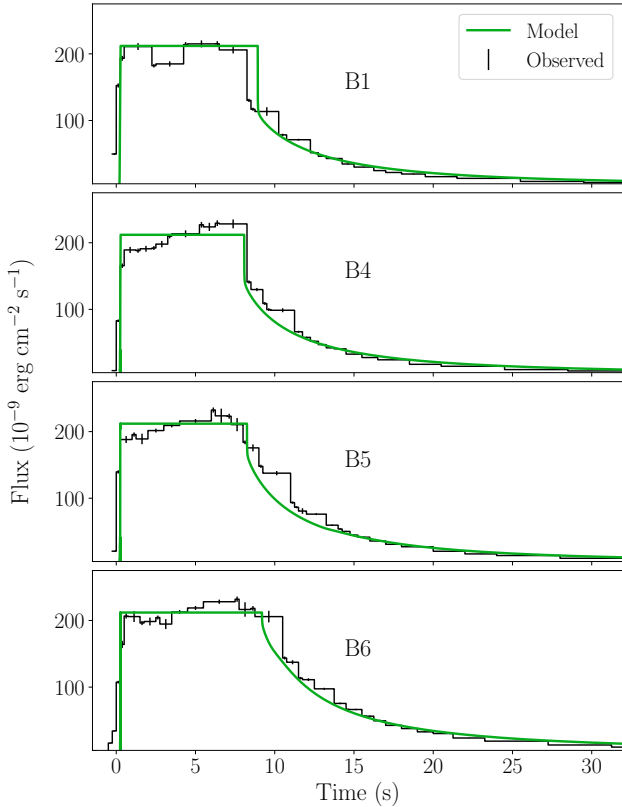


Figure 4. The lightcurves for each modelled burst (solid green curve) against its observed counterpart (black bins). The model luminosity has been converted to an observed flux using the scaling factor $c_2 = 4\pi d^2 \xi_b = 1.05 \times 10^{45} \text{ cm}^2$, chosen such that the burst fluences best match the observations (§ 3.2).

2.6 Burst properties

We ran KEPLER with the above inputs, and obtained a sequence of bursts over the course of the outburst. We then extracted the burst lightcurves from the modelled NS surface luminosity, and calculated their properties in a process similar to Lampe et al. (2016).

The recurrence time, Δt , is the time from one burst to the next. The burst energy, E_{nuc} , is obtained by integrating over the lightcurve. This translates to the observed burst fluence, E_b , via

$$E_b = \frac{1}{4\pi d^2 \xi_b} E_{\text{nuc}}. \quad (8)$$

Similar to Equation 7, this expression can also be written in terms of a scaling factor,

$$E_b = \frac{1}{c_2} E_{\text{nuc}} \quad \text{with} \quad c_2 = 4\pi d^2 \xi_b. \quad (9)$$

The profiles of PRE burst lightcurves in KEPLER noticeably deviate from observations, likely due to the simple atmosphere (see Model Z_m in Woosley et al. 2004). In our model, the surface luminosity exceeded the Eddington limit by up to a factor of two, followed by a steep drop (Fig. 2). Luminosity in excess of Eddington should drive further radius expansion, or even be converted into a wind, a mechanism which these models lack. In order to compare

our results with observations, we manually truncated the lightcurves at the Eddington luminosity for pure helium, $L_{\text{Edd}} = 3.53 \times 10^{38} \text{ erg s}^{-1}$, the inferred limit reached for PRE bursts (Kuulkers et al. 2003).

3 RESULTS

We present here a model which closely reproduced the observed burst times. We must emphasise that we present this not as a best-fitting model to the observations, but to demonstrate the feasibility of modelling bursts under varying accretion rates. A more detailed and systematic exploration of model parameters is planned as a future study.

The model produced a sequence of ten X-ray bursts over the course of the outburst (Table 2, Fig. 3). The bursts have been assigned labels to aid in discussion. Seven are labelled sequentially from B1 to B7, where B1 is the closest in time to the first observed burst. The observed bursts are labelled O1, O4, O5, and O6, to correspond with their closest model bursts. Three bursts occur prior to B1, and are labelled P1, P2, and P3, in reverse order from B1, in anticipation of future simulations which may produce more or fewer such bursts.

We have applied GR corrections to the modelled burst properties, such that they correspond to a distant observer (§ 2.3). Error bars for the observational data are 1σ uncertainties. We have set the model uncertainties to 3 percent, which is the typical 1σ variation in modelled burst trains when all input parameters (including \dot{M}) are held constant (§ 3.1). The uncertainties in the modelled burst arrival times were obtained by propagating the 3 percent uncertainty in Δt along the burst train (the uncertainty for the first burst was simply taken to be that of the following recurrence interval). Additional model uncertainties due to the observational uncertainties in distance, inclination etc. are not considered for the purpose of this paper, because we are not yet attempting parameter estimation.

3.1 Varying versus averaged accretion rates

We performed a comparison test in order to check for any difference in results between a varying and an averaged accretion rate. For each burst interval in the model, Δt_v , we calculated the average accretion rate, $\langle \dot{M} \rangle$. We then independently restarted the simulation at the beginning of each interval, with \dot{M} now fixed at $\langle \dot{M} \rangle$. Once a sequence of 10–15 bursts were produced at each $\langle \dot{M} \rangle$, we calculated the mean recurrence times, $\langle \Delta t \rangle$. We then compared these with the original recurrence times, Δt_v , and calculated the average slope of $\dot{M}(t)$ for each interval, given by $\Delta \dot{M} / \Delta t_v$ (Fig. 5). The standard deviation in burst properties for each $\langle \Delta t \rangle$ was typically ≈ 3 percent, and we have adopted this as the standard model uncertainty. We have excluded the first burst interval (P3-P2) from this comparison because it is abnormally short, with a recurrence time almost half the length of the next, despite a lower accretion rate. We attribute this to extra heating from the very large preceding burst, P3.

The variables $\langle \Delta t \rangle / \Delta t_v$ and $\Delta \dot{M} / \Delta t_v$ have a Spearman’s rank correlation coefficient of $r_s = 0.60$, with a p -value of $p = 0.12$. A least-squares linear regression, weighted

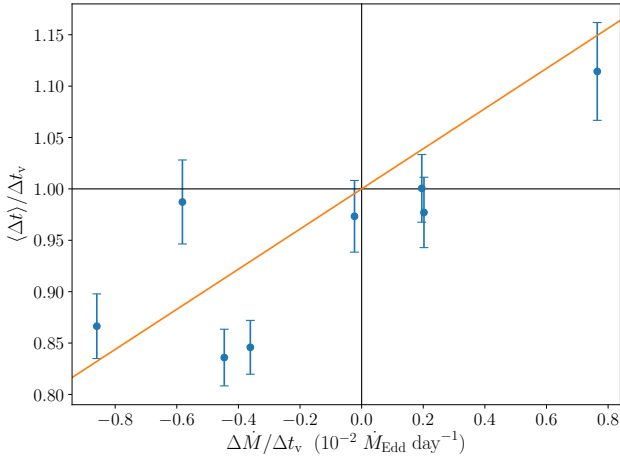


Figure 5. The result of using a constant $\langle \dot{M} \rangle$ in place of a varying $\dot{M}(t)$. The vertical axis is the ratio of the recurrence time from a constant accretion rate ($\langle \Delta t \rangle$) to the recurrence time from a varying accretion rate (Δt_v). On the horizontal axis is the average slope of $\dot{M}(t)$ for the interval. The trendline is a weighted least-squares regression that has been forced through the point (0, 1), and has a slope of 0.195.

with the uncertainties and forced through the point (0, 1), returns a slope of 0.195. The correlation appears to have a low significance, although it is somewhat inconclusive with such a small sample. The scatter may be due in part to the small-scale variations in $\dot{M}(t)$ within each interval, given that $\Delta \dot{M} / \Delta t_v$ is itself an approximation to the slope. Nevertheless, this tentatively suggests that using a constant $\langle \dot{M} \rangle$ may systematically overestimate Δt_v when $\dot{M}(t)$ is increasing, and underestimate Δt_v when $\dot{M}(t)$ is decreasing. This discrepancy could have a significant effect on predictions, because burst properties are strongly dependent on the recurrence time. It's possible that the relationship is dependent on other parameters such as Q_b , X_0 and Z_{CNO} . With further study, a correction factor could account for this systematic discrepancy when an averaged accretion rate can't be avoided, as with the semi-analytic models of G06.

3.2 Comparison with observed bursts

The four observed burst times are matched to within 0.85 h, 0.27 h, 1.8 h, and 5.4 h, respectively. The RMS error for the four bursts is 2.88 h, in comparison to their recurrence times of $18 \lesssim \Delta t \lesssim 33$ h. An additional source of discrepancy here may be the gaps in PCA data. Because we have used linear interpolation in the PCA gaps, any unobserved variation in \dot{M} is not captured in the model.

Six extra bursts were predicted in addition to the four observed. Three of these (P1 – P3) were during the accretion rise, preceding O1. Two intervening bursts (B2, B3) fell between O1 and O4, and a final burst (B7) fell during the outburst tail, ≈ 2.5 days after O6. All extra bursts fell within gaps in the PCA data, and so can't immediately be ruled out by observations. The two intervening bursts, B2 and B3, agree with the predictions of G06, who concluded that two bursts likely occurred between O1 and O4. Our model also suggests that several other bursts may have been missed.

Table 2. Burst properties for the model with $X_0 = 0.44$ (for a description of burst labels, see § 3). Observed bursts and their modelled counterparts are highlighted in bold.

Burst	t (h)	Δt (h)	E_b (10^{-6} erg cm $^{-2}$)
P3	-33.1 ± 0.3	—	11.0 ± 0.3
P2	-24.7 ± 0.3	8.4 ± 0.3	2.11 ± 0.06
P1	-8.6 ± 0.5	16.1 ± 0.5	2.57 ± 0.08
B1	9.0 ± 0.8	17.6 ± 0.5	2.73 ± 0.08
O1	8.2*	—	2.620 ± 0.021
B2	22.7 ± 0.9	13.6 ± 0.4	2.53 ± 0.08
B3	35.6 ± 0.9	12.9 ± 0.4	2.45 ± 0.07
B4	53.3 ± 1.1	$44.3 \pm 0.8^\dagger$	2.67 ± 0.08
O4	53.6	45.4	2.649 ± 0.018
B5	76.5 ± 1.3	23.2 ± 0.7	2.89 ± 0.09
O5	74.7	21.1	2.990 ± 0.017
B6	109.9 ± 1.6	33.4 ± 1.0	3.44 ± 0.10
O6	104.5	29.8	3.460 ± 0.022
B7	165 ± 2	54.6 ± 1.6	4.34 ± 0.13

*Observational time uncertainties are < 1 s and are excluded for clarity

† Total interval between B1–B4, to compare with the observed value.

When converted from E_{nuc} via Equation 9, the burst fluences, E_b , have a minimised RMS error with the observations when $c_2 \approx 1.05 \times 10^{45}$ cm 2 . Following this scaling, the RMS error of the four bursts is 0.11×10^{-6} erg cm $^{-2}$, in comparison to their fluence range of $2.7 \lesssim E_b \lesssim 3.4$ erg cm $^{-2}$. Overall, the model reproduces the observed trend of increasing E_b with recurrence time (Fig. 3). This is consistent with larger fuel layers accumulating due to a lowering accretion rate and a cooling envelope.

From Equation 7 and Equation 9, we have

$$\frac{\xi_p}{\xi_b} = \frac{c_1}{c_2}, \quad (10)$$

$$d = \sqrt{\frac{c_1}{4\pi\xi_p}} = \sqrt{\frac{c_2}{4\pi\xi_b}}, \quad (11)$$

where for this model $c_1/c_2 \approx 1.536$. According to the thin accretion disc model from He & Keek (2016, Model a), this anisotropy ratio occurs at an inclination of $i = 67.7^\circ$, with $\xi_p = 1.85$ and $\xi_b = 1.21$. Using Equation 11, this corresponds to a distance of $d = 2.7$ kpc, which is outside the range proposed by G06 of 3.5 ± 0.1 kpc. This may be due to the inherent differences between the models, that the anisotropy was not considered in their study, or because our model is not yet a global best fit to the system. Additionally, a thin accretion disc may not be realistic for a transiently accreting LMXB, and other disc geometries produce different relationships between ξ_p and ξ_b . For instance, a concave disc (Model d of He & Keek 2016) predicts the same anisotropy ratio at $i = 62.6^\circ$, with $\xi_p = 1.34$ and $\xi_b = 1.10$, corresponding to a distance of $d = 3.1$ kpc, closer to the accepted value.

Following Eddington-truncation and scaling, the burst

lightcurves broadly reproduce the observed profiles, featuring sharp rise times and gradual decays (Fig. 4). The plateau peak has been fixed at L_{Edd} , and after scaling c_2 to match the observed E_b , it approximately agrees with the observed peaks.

4 CONCLUSION

We performed simulations of a neutron star envelope during an accretion outburst, using the time-dependent $\dot{M}(t)$ inferred from the 2002 October event of SAX J1808.4-3658. A composition of $Z_{\text{CNO}} = 0.02$ and $X_0 = 0.44$ reproduced the four observed burst arrival times with a RMS error of 2.88 h, with recurrence times of $18 \lesssim \Delta t \lesssim 33$ h. The modelled sequence contained ten bursts, six of which did not correspond to observed bursts: three during the accretion rise; two between the first and second observed bursts; and one during the tail, ≈ 2.5 days after the fourth observed burst. These extra bursts fell during times when the source was not being observed by *RXTE*, which had a duty cycle of 38 percent for the outburst.

Due to the limitations of KEPLER when simulating PRE bursts, the model-predicted luminosities were manually truncated at L_{Edd} in order to compare other lightcurve features to observations. The lightcurves have rapid rise times (< 1 s) and fast decays (≈ 20 s), in agreement with the observed characteristics of helium-rich bursts. The burst fluences were reproduced with a RMS error of $0.11 \times 10^{-6} \text{ erg cm}^{-2}$ after scaling by $c_2 = 4\pi d^2 \xi_b \approx 1.05 \times 10^{45} \text{ cm}^2$.

To obtain similar recurrence times to the best-fitting models of G06, we required a lower hydrogen fraction of $X_0 = 0.44$, in comparison to $X_0 = 0.54$. A difference is perhaps unsurprising given the degrees of complexity between the models. For example, the semi-analytic model of G06 solves for thermonuclear stability with a one-zone approximation, does not evolve bursts with time, and uses a simple expression for energy yield to calculate the total burst energy. Furthermore, our results suggest that using averaged accretion rates may overestimate the recurrence times for an increasing \dot{M} , and underestimate recurrence times for a decreasing \dot{M} . Efforts are currently underway to improve the semi-analytic model of G06 and its application to the 2002 October outburst.

As mentioned, the model presented here is not yet a global fit to the data, and so posterior constraints on the system parameters are not yet possible. In a future study, a more systematic matching could be performed by varying Z_{CNO} , Q_b , \dot{M} , R , c_1 , c_2 , and the assumed accretion onset. The strength of the crustal heating, Q_b , may itself evolve with \dot{M} . In addition to the burst times, other properties such as the peak luminosities, lightcurve profiles, and E_b could be incorporated into the fitting routine to obtain a global likelihood value.

Matching the properties of multiple bursts over a single accretion event provides a new test bed for multi-zone models. Our simulations are the first to adopt a time-dependent \dot{M} , and demonstrate that existing burst models can be extended to transient accretion regimes. This may help to further constrain LMXB properties, including the NS mass and radius, the strength of crustal heating, and the distance and

inclination of the system. Furthermore, constraining the fuel composition provides information about the composition of the companion star, and thus the evolutionary history of the binary. This could improve our understanding of the SAX J1808.4-3658 system, and more generally, the origin of accreting millisecond pulsars.

ACKNOWLEDGEMENTS

This work was supported in part by the National Science Foundation under Grant No. PHY-1430152 (JINA Center for the Evolution of the Elements). This research was supported by an Australian Government Research Training Program (RTP) Scholarship. This paper utilises preliminary analysis results from the Multi-INstrument Burst Archive (MINBAR), which is supported under the Australian Academy of Science's Scientific Visits to Europe program, and the Australian Research Council's Discovery Projects and Future Fellowship funding schemes. This research was supported in part by the Monash eResearch Centre and eSolutions-Research Support Services through the use of the MonARCH HPC Cluster. We thank Jordan He and Laurens Keek for providing data tables from their disc anisotropy models described in He & Keek (2016), and Andrew Cumming and Adelle Goodwin for discussions about the analytic model used in G06. AH was supported by an ARC Future Fellowship (FT120100363). ZJ would like to thank Michigan State University for their generous hospitality on a research visit, during which this manuscript was partially prepared.

REFERENCES

- Belian R. D., Conner J. P., Evans W. D., 1976, *The Astrophysical Journal Letters*, 206, L135
- Bildsten L., Chakrabarty D., 2001, *The Astrophysical Journal*, 557, 292
- Chakrabarty D., Morgan E. H., 1998, *Nature*, 394, 346
- Chakrabarty D., Morgan E. H., Muno M. P., Galloway D. K., Wijnands R., van der Klis M., Markwardt C. B., 2003, *Nature*, 424, 42
- Cumming A., Bildsten L., 2000, *The Astrophysical Journal*, 544, 453
- Cyburt R. H., et al., 2010, *The Astrophysical Journal Supplement Series*, 189, 240
- Cyburt R. H., Amthor A. M., Heger A., Johnson E., Keek L., Meisel Z., Schatz H., Smith K., 2016, *The Astrophysical Journal*, 830, 55
- Dorman B., Arnaud K. A., 2001. p. 415, <http://adsabs.harvard.edu/abs/2001ASPC...238..415D>
- Fujimoto M. Y., 1988, *The Astrophysical Journal*, 324, 995
- Fujimoto M. Y., Hanawa T., Miyaji S., 1981, *The Astrophysical Journal*, 247, 267
- Galloway D. K., 2006, [arXiv:astro-ph/0604345](https://arxiv.org/abs/astro-ph/0604345), 840, 50
- Galloway D. K., Cumming A., 2006, *The Astrophysical Journal*, 652, 559
- Galloway D. K., Muno M. P., Hartman J. M., Psaltis D., Chakrabarty D., 2008, *The Astrophysical Journal Supplement Series*, 179, 360
- Galloway D. K., Goodwin A. J., Keek L., 2017, *Publications of the Astronomical Society of Australia*, 34, e019
- Grindlay J., Gursky H., Schnopper H., Parsignault D. R., Heise J.,

- Brinkman A. C., Schrijver J., 1976, *The Astrophysical Journal Letters*, 205, L127
- Hartman J. M., et al., 2008, *The Astrophysical Journal*, 675, 1468
- Hartman J. M., Watts A. L., Chakrabarty D., 2009, *The Astrophysical Journal*, 697, 2102
- He C.-C., Keek L., 2016, *The Astrophysical Journal*, 819, 47
- Heger A., Langer N., Woosley S. E., 2000, *The Astrophysical Journal*, 528, 368
- Heger A., Cumming A., Galloway D. K., Woosley S. E., 2007, *The Astrophysical Journal Letters*, 671, L141
- Ibragimov A., Poutanen J., 2009, *Monthly Notices of the Royal Astronomical Society*, 400, 492
- Jahoda K., Swank J. H., Giles A. B., Stark M. J., Strohmayer T., Zhang W. W., Morgan E. H., 1996. International Society for Optics and Photonics, pp 59–71, doi:10.1117/12.256034
- Joss P. C., 1977, *Nature*, 270, 310
- Keek L., Heger A., 2011, *The Astrophysical Journal*, 743, 189
- Kuulkers E., den Hartog P. R., in't Zand J. J. M., Verbunt F. W. M., Harris W. E., Cocchi M., 2003, *Astronomy and Astrophysics*, 399, 663
- Lampe N., Heger A., Galloway D. K., 2016, *The Astrophysical Journal*, 819, 46
- Levine A. M., Bradt H., Cui W., Jernigan J. G., Morgan E. H., Remillard R., Shirey R. E., Smith D. A., 1996, *The Astrophysical Journal Letters*, 469, L33
- Lewin W. H. G., Vacca W. D., Basinska E. M., 1984, *The Astrophysical Journal*, 277, L57
- Lewin W. H. G., Paradijs J. V., Taam R. E., 1993, *Space Science Reviews*, 62, 223
- Patruno A., Watts A. L., 2012, preprint, 1206, arXiv:1206.2727
- Patruno A., Bult P., Gopakumar A., Hartman J. M., Wijnands R., van der Klis M., Chakrabarty D., 2012, *The Astrophysical Journal Letters*, 746, L27
- Patruno A., et al., 2017, *The Astrophysical Journal*, 841, 98
- Rauscher T., Heger A., Hoffman R. D., Woosley S. E., 2002, *The Astrophysical Journal*, 576, 323
- Strohmayer T., Bildsten L., 2003, arXiv:astro-ph/0301544
- Tawara Y., et al., 1984, *The Astrophysical Journal*, 276, L41
- Ubertini P., Bazzano A., Cocchi M., Natalucci L., Heise J., Muller J. M., in 't Zand J. J. M., 1999, *The Astrophysical Journal Letters*, 514, L27
- Wang Z., et al., 2001, *The Astrophysical Journal Letters*, 563, L61
- Weaver T. A., Zimmerman G. B., Woosley S. E., 1978, *The Astrophysical Journal*, 225, 1021
- Wijnands R., 2004, *Nuclear Physics B Proceedings Supplements*, 132, 496
- Wijnands R., van der Klis M., 1998, *Nature*, 394, 344
- Woosley S. E., Taam R. E., 1976, *Nature*, 263, 101
- Woosley S. E., et al., 2004, *The Astrophysical Journal Supplement Series*, 151, 75
- in 't Zand J. J. M., Heise J., Muller J. M., Bazzano A., Cocchi M., Natalucci L., Ubertini P., 1998, *Astronomy and Astrophysics*, 331, L25

This paper has been typeset from a $\text{\TeX}/\text{\LaTeX}$ file prepared by the author.